Review

The Charging-Up Phenomenon in Gas Electron Multiplier Detector

Sayak Chatterjee *, Supriya Das, Saikat Biswas

Posted Date: 20 March 2026

doi: 10.20944/preprints202603.1620.v1

Keywords: micro pattern gas detector (MPGD); gas electron multiplier (GEM); charging-up; dielectric polarisation; charging-up time; uniformity; gain; energy resolution; count rate; radioactive source; Monte Carlo (MC) simulation

 doi:10.20944/preprints202603.1620.v1

Review

The Charging-Up Phenomenon in Gas Electron Multiplier Detector

Sayak Chatterjee [1,*], Supriya Das [2] and Saikat Biswas [2]

[1] Department of Physics, University of Massachusetts, Amherst, USA
[2] Department of Physical Sciences, Bose Institute, Kolkata, India
* Correspondence: sayakchatterjee896@gmail.com

Abstract

Fabio Sauli introduced Gas Electron Multiplier (GEM) technology in 1997, which has since evolved into one of the most versatile and widely adopted micro pattern gaseous detector (MPGD) technologies for tracking in High Energy Physics (HEP) experiments. Owing to its high rate-handling capability ($\sim$ MHz/mm^2), good position resolution ($\sim$ 100 μm), and operational robustness in high radiation environments. GEM detectors have become an indispensable component of modern tracking systems. The heart of a GEM detector is a thin Kapton polyimide foil ($\sim$ 50 μm) clad with copper ($\sim$ 5 μm) on both sides and containing an array of regularly spaced holes (typically diameter of $\sim$ 70 μm and pitch of $\sim$ 140 μm) fabricated using photolithographic techniques. The presence of the dielectric substrate (Kapton) within the amplification region introduces a time dependent response when the detector is exposed to external irradiation, a phenomenon commonly referred to as the charging-up effect. This effect arises from the accumulation of charge on the insulating Kapton surfaces, leading to a gradual modification of the local electric field configuration inside the GEM holes and, consequently, a variation in the detector gain over time. The charging-up behaviour has been systematically investigated for triple GEM chamber prototypes using an Fe-55 radioactive source (5.9 keV X-rays). The characteristic charging-up time constant has been extracted, and its dependence on detector gain and irradiation rate has been examined. In addition, the uniformity of detector performance in terms of count rate, gain, and energy resolution has been studied both before and after the charging-up process. In this review article, the experimental setup, data acquisition methodology, and analysis procedures developed and carried out by our group are summarised. The key findings reported by other groups, relevant Monte Carlo simulation efforts, and future outlook for the charging-up investigation on GEM based detectors are also discussed in this article. The investigations and their outcomes reviewed here provide valuable insight into the charging-up dynamics of GEM detectors and their dependence on operational parameters.

Keywords: micro pattern gas detector (MPGD); gas electron multiplier (GEM); charging-up; dielectric polarisation; charging-up time; uniformity; gain; energy resolution; count rate; radioactive source; Monte Carlo (MC) simulation

1. Introduction

Fabio Sauli introduced Gas Electron Multiplier (GEM) technology in 1997 [1], which has since evolved into one of the most versatile and widely adopted micro pattern gaseous detector (MPGD) technologies in High Energy Physics (HEP) experiments [2,3] for tracking. Owing to its capability of handling high rates ($\sim$ MHz/mm^2), operational robustness in high radiation environments, and good position resolution ($\sim$ 100 μm), GEM detectors have become an indispensable component of modern tracking systems [4]. They have been successfully deployed in several large scale experiments such as COMPASS [4–6], ALICE [7,8], and CMS [9,10] at CERN, ePHENIX (RHIC) [11] at Brookhaven National Laboratory (BNL), the Super BigBite Spectrometer (SBS) [12] program at Jefferson Laboratory (JLab),

 doi:10.20944/preprints202603.1620.v1

etc. Furthermore, GEM based systems are proposed for future experiments, including CBM [13,14] at FAIR, SoLID [15] at JLab, the Electron-Ion Collider (EIC) [16,17] at BNL, and NA60+ [18,19] at CERN. Beyond the domain of particle physics, GEM detectors are increasingly being utilised in applied fields such as muon tomography, security imaging, medical diagnostics, etc., underscoring their versatility and adaptability [20–27].

The heart of a GEM detector is thin Kapton polyimide foils ($\sim 50\ \mu$m) clad with copper ($\sim 5\ \mu$m) on both sides and perforated with a high density (typically 50–100 mm^{-2}) of holes [1]. Usually, the diameter of the holes is $\sim 70\ \mu$m and the pitch is $\sim 140\ \mu$m [1]. In Figure 1, typical electric field lines (left) inside and around the GEM foils and a microscope image of the foil (right) are shown. The holes in the copper clad Kapton foil are created through a photolithographic technique [28]. Depending on the fabrication process, GEM foils are categorised as either double mask (DM) or single mask (SM) types. One of the main differences between the DM and SM techniques lies in the masking of the copper clad Kapton foil to define the hole patterns and the subsequent etching of the foil. As the name suggests, in the DM technique the masking is performed on both sides of the copper clad Kapton film, and etching is carried out isotropically from both directions, resulting in bi-conical holes. However, for larger GEM foils (with dimensions > 40 cm $\times$ 40 cm), it is very difficult to align the top and bottom masks to the desired precision, which can lead to the formation of slanted holes. This limitation motivated the development of the SM technique, in which the masking is performed only on one side and etching is carried out from that side where the hole patterns are engraved. Asymmetrical holes are formed because of the etching from one end, and consequently the detector performance depends on the orientation of GEM foils produced using the SM technique. Several studies have been carried out to understand the effect of GEM hole geometry on detector performance [29–31].

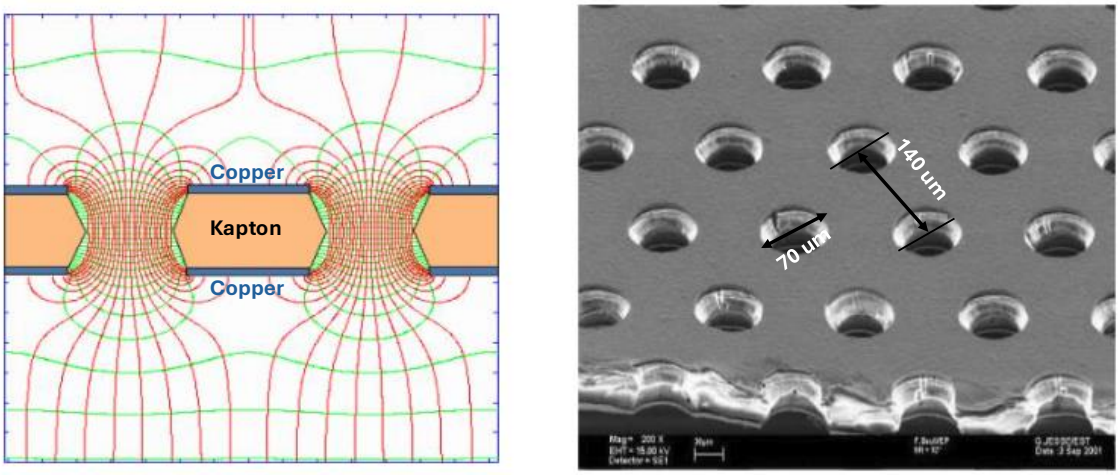

Figure 1. (Left:) Electric field lines inside and around the GEM holes. (Right:) GEM foil under a microscope. The diameter of the holes is typically $\sim 70\ \mu$m, and the pitch is $\sim 140\ \mu$m [32].

The basic operating principle of this detector is accurately reflected in its name, as it multiplies the electrons produced by the interaction of incoming charged particles with the gas molecules in the detector's active area through the application of a strong electric field gradient. In a typical GEM detector, an electrode placed at the top is referred to as the drift electrode, while a charge collection electrode placed at the bottom to collect the produced charges is referred to as the readout plane. High voltage (HV) is applied externally to generate the required electric field in the active area of the

 doi:10.20944/preprints202603.1620.v1

detector. In the case of a triple GEM chamber, three GEM foils are placed between the drift electrode and the readout plane. A schematic of a triple GEM detector is shown in Figure 2 [33,34].

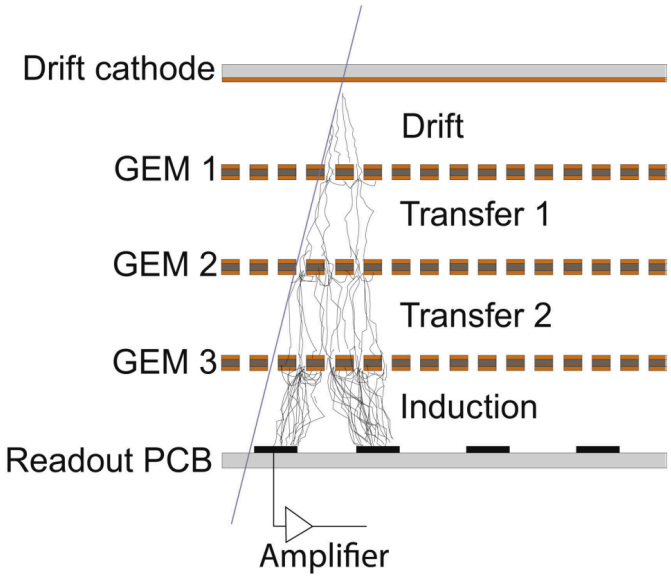

Figure 2. Schematic of a triple GEM detector showing the different regions of the chamber [33].

The region between the drift electrode and the first GEM foil is called the drift gap. The gaps between individual GEM foils are referred to as transfer gaps. The region between the last GEM foil and the readout plane is known as the induction gap. For a chamber containing three GEM foils, also known as the triple GEM chamber, the gap between the first and second GEM foils is called transfer gap 1, while transfer gap 2 is the region between the second and third GEM foils. The drift, transfer, and induction gaps have been optimised through dedicated R&D and are typically set to 3 mm, 2 mm, 2 mm, and 2 mm, respectively, for general use of the triple GEM detector [1,2]. This configuration is commonly referred to as the 3-2-2-2 configuration. Primary ionisation usually occurs in the drift region of the detector due to the interaction of incoming charged particles with the gas molecules, producing primary electron–ion pairs. These primary electrons are then guided toward the first GEM foil by the drift field (typically 2–4 kV/cm) generated by the potential difference between the drift electrode and the top of the first GEM foil. A typical potential difference of ∼400 V is applied across a GEM foil to create a high electric field, typically ∼80 kV/cm, inside the GEM holes. Due to the presence of this high electric field, incoming electrons gain sufficient energy to ionise additional gas molecules, resulting in an electron avalanche. After the avalanche, a large fraction of the electrons exit the multiplication region and enters the next stage of the detector, where they can either be collected, in the case of a single GEM, or guided into subsequent multiplication layers in detectors employing multiple GEM foils. The fraction of electrons exiting the multiplication region also depends on the strength of the electric field in the subsequent region. The gain of the detector is defined as the ratio of the number of electrons reaching the readout plane to the number of electrons produced during primary ionisation in the drift region. One of the main advantages of GEM detectors is that they can be operated in cascade mode, where multiple GEM foils are stacked to assemble a chamber. This configuration not only increases the detector gain at relatively lower applied voltages, thereby improving the signal to noise ratio, but also reduces the discharge probability, since the discharge probability in GEM detectors increases with gain, which is proportional to the applied voltage [2,33,34].

The choice of the number of GEM layers, gas gap configuration, and gas mixture as the active medium depends on the experimental requirements. For example, GEM chambers have been operated with an Ar/CO_2 gas mixture in a 70/30 volume ratio as tracking devices in COMPASS (3-2-2 configuration) [4–6], CMS (3-1-2-1 configuration) [9,10] , and TOTEM (3-2-2-1 configuration) [36,37]. For the ALICE TPC readout, a special type of quadrupole GEM chambers (2-2-2-2-2 configuration) have

 doi:10.20944/preprints202603.1620.v1

been used with $Ne/CO_2/N_2$ gas mixture in the ratio of 90/10/5, where the primary objective was to reduce ion backflow [7,8]. At LHCb, triple GEM chambers (3-1-2-1 configuration) have been used as triggering devices and operated with $Ar/CO_2/CF_4$ gas mixture in the ratio of 45/15/40 [38,39].

GEM technology is also gaining popularity outside high and intermediate energy nuclear physics experiments, including applications such as muon tomography, gamma-ray polarimetry, neutron detection, and medical diagnostics [20–27].

Despite these achievements, investigating the performance of GEM detectors under prolonged and harsh radiation environments remains an active area of research, particularly to understand radiation induced effects more thoroughly. The charging-up effect is one such radiation induced phenomenon, where the presence of the dielectric substrate (Kapton) within the amplification region of the chamber introduces a time dependent response when the detector is exposed to external irradiation. This effect arises from the accumulation of charge on the insulating surfaces of the Kapton foil, leading to a gradual modification of the local electric field configuration inside the GEM holes and a corresponding variation in the effective gain over time [40–50]. In Section 2, a brief overview of the charging-up phenomenon in GEM detectors is provided. Section 3 presents an overview of the experimental setup and data-taking methodology developed by the authors. The observations on the charging-up effect in different GEM chamber prototypes are discussed in Section 4. A brief summary of related experimental efforts by other groups are also presented towards the end of the Section 4. A brief summary of Monte Carlo (MC) simulation efforts by different groups to model the charging-up phenomenon is provided in Section 5. Finally, Section 6 summarises the findings and outlines potential future steps to further improve the understanding of the charging-up phenomenon in GEM detectors.

2. The Charging-Up Phenomenon in GEM Detector

The change in detector gain under external irradiation, due to the presence of Kapton in the active volume, is referred to as the charging-up effect. In Figure 3 [45], a schematic cross-sectional view of a GEM hole is shown along with the applied potential and the direction of the electric field lines. Usually, the potential is applied such that the top of the GEM plane remains at a negative potential relative to the bottom of the GEM foil, ensuring that electrons drift toward the readout plane while ions move in the opposite direction. Due to the applied voltage, the dielectric polyimide (Kapton) becomes polarised, and the induced electric field resulting from dielectric polarisation is shown in Figure 3 as $E_{Polarised}$.

 doi:10.20944/preprints202603.1620.v1

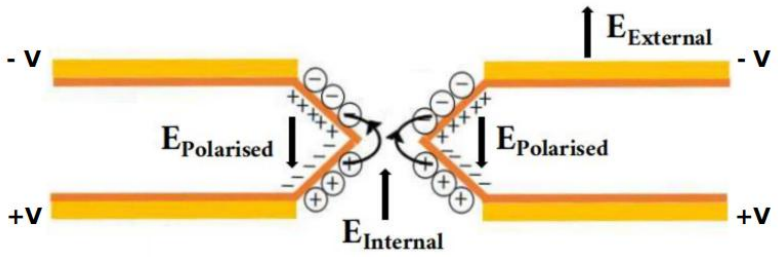

Figure 3. Schematic illustration of the charging-up effect inside a GEM hole. $E_{External}$ denotes the field generated by the applied high voltage. $E_{Polarised}$ denotes the electric field generated due to the polarisation of the dielectric medium (Kapton), and $E_{Internal}$ is the field generated by the accumulation of charges on the dielectric (Kapton) surface, creating a lensing effect and thereby increasing the electric field strength inside the GEM hole [45].

The high electric field inside the GEM holes, created by the potential difference across the GEM foil, facilitates the development of an avalanche of further ionisation within the hole, producing additional electron–ion pairs. During this multiplication process, the generated electrons and ions diffuse toward the polyimide surface, and since the surface is already polarised, a fraction of these charges becomes adsorbed onto the Kapton surface. These charges remain on the dielectric surface for relatively long times due to the high resistivity of Kapton, eventually forming a layer of electron–ion pairs on the surface, as shown in Figure 3. The accumulation of charge on the Kapton walls dynamically modifies the electric field inside the GEM hole, acting as a lensing effect and thereby strengthening the electric field within the hole. In Figure 3, it is shown that the electric field generated by the accumulated charges on the Kapton surface ($E_{Internal}$) acts in the same direction as the external field ($E_{External}$) generated by the applied voltage. As a result, the detector gain increases during the initial phase of operation and then asymptotically approaches a constant value as charge accumulation on the Kapton surface reaches a dynamic equilibrium. Therefore, detector gain is a key observable for understanding the effect of charging-up on detector response under external irradiation.

A series of systematic studies has been carried out at Bose Institute, Kolkata, India, to investigate the charging-up phenomenon in both SM and DM triple GEM chamber prototypes of dimension 10 cm $\times$ 10 cm using an Fe-55 radioactive X-ray source with characteristic energy of 5.9 keV [44–46]. A single Fe-55 radiation source served the dual purpose of irradiating the chamber and acquisition of the energy spectrum. The temporal evolution of detector gain has been analysed, and the initial charging phase has been modelled using an exponential function, drawing an analogy with the charging behaviour of a resistive-capacitive (RC) network [51]. The characteristic charging-up time constant has been extracted, and its dependence on detector gain and irradiation rate has been examined [44,45]. In addition, the uniformity of detector performance in terms of count rate, gain, and energy resolution has been studied both before and after the charging-up process [46]. For all studies, the chambers were operated in continuous flow mode with an Ar/CO_2 gas mixture in a 70/30 volume ratio.

These measurements provide valuable insight into the charging dynamics of GEM detectors and their dependence on operational parameters. A detailed description of the experimental setup, data acquisition methodology, analysis procedures, and observed results by the authors is presented in the following section. A brief summary of findings from other groups on GEM charging-up investigations is also included toward the end of the following section.

 doi:10.20944/preprints202603.1620.v1

3. Experimental Setup

A dedicated setup has been developed at Bose Institute, Kolkata, India, to study radiation induced effects in gas-filled detectors, in particular GEM [52–62], Resistive Plate Chambers (RPCs) [63–69], and straw-tube [70–74] detector prototypes, by investigating their long-term performance stability, ageing, and efficiency under external irradiation. Different radioactive sources have been used for irradiation. For the charging-up studies, triple GEM chamber prototypes of both DM [45] and SM [44,46] types, each with dimensions of 10 cm $\times$ 10 cm, have been used with a Fe-55 X-ray source ($\sim$20 mCi) with a characteristic energy of 5.9 keV. Both detectors were operated with Ar/CO_2 gas mixture in continuous flow mode at a typical flow rate of $\sim$3 l/hr. Standard NIM electronics have been used for data acquisition, and the data have been analysed using the CERN ROOT framework [75].

3.1. Detector Description

In Figure 4 (left), the schematic of the voltage divider network for the DM triple GEM chamber under investigation is shown [45]. A similar voltage divider network has been used for the SM triple GEM detector prototype [44], along with an HV filter [1] placed between the drift plane and the HV input.

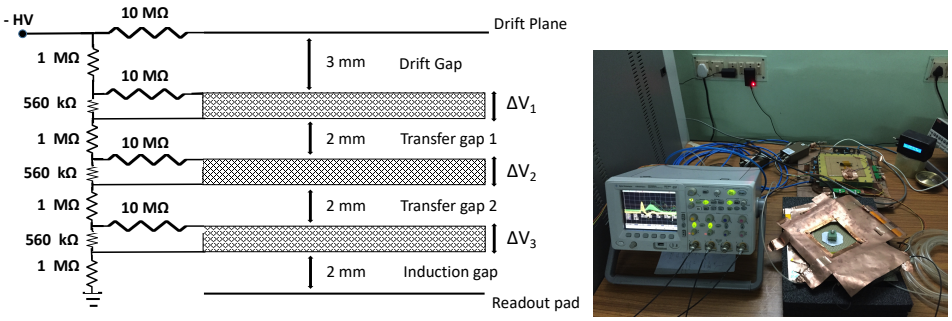

Figure 4. (Left:) Schematic of the voltage divider network for the DM triple GEM detector prototype under investigation. (Right:) The experimental setup of the prototype DM triple GEM chamber exposed to an Fe-55 source. The raw signal (yellow band) and the amplified signal (green band) from the detector are shown on the oscilloscope.

The typical signal from the DM triple GEM detector using an Fe-55 source can be seen on the oscilloscope in Figure 4 (right). Both detector prototypes under study have a 3-2-2-2 configuration. A 10 MΩ protection resistor has been used with the drift plane as well as with the top of each GEM foil. The readout of the DM detector prototype consisted of nine pads, each with dimensions of 9 mm $\times$ 9 mm, placed at the centre of the active area of the detector. For the SM detector prototype, the readout consisted of an XY printed circuit board with 256 X and 256 Y tracks. Each set of XY tracks has been connected to 128-pin connectors. Sum-up boards have been used to combine the signals from the readout pads (DM triple GEM chamber) or strips (SM triple GEM chamber) before further signal processing. For the DM GEM detector prototype, a single sum-up board has been used, while for the SM GEM detector prototype, four sum-up boards have been employed. The circuit diagram used for signal counting and spectrum storage is shown in Figure 5.

[1] An RC circuit with a 1 MΩ resistor and a 2.2 nF capacitor connected in series to act as a low-pass filter. This was added to block any AC components that might be present in the HV line.

 doi:10.20944/preprints202603.1620.v1

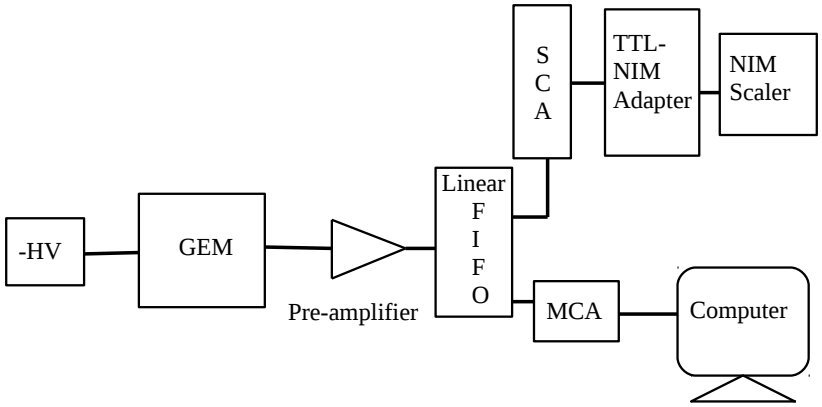

Figure 5. Schematic for the electronic setup of the data acquisition system.

Negative high voltage has been applied to the drift plane and distributed to the different sections of the detector. The signal from the sum-up board has been fed into a charge-sensitive preamplifier (VV50-2) [76] with a gain of 2 mV/fC and a shaping time of 300 ns. The output signal from the preamplifier has then been fed into a linear fan-in fan-out (FIFO) module, which generates identical copies of the input analogue signal. One analogue output from the FIFO has been fed into a single channel analyser (SCA) operated in integral mode, where the lower level discriminator has been used as the signal threshold. The discriminated output from the SCA, which was TTL[2] in nature, has been sent to a TTL–NIM adapter, which converts the TTL signal into a NIM[3] signal and a NIM scaler was used to count the signal. Another output from the FIFO module has been fed into a multi-channel analyser (MCA) to store the energy spectra from the detector on a computer. These spectra have been analysed offline to extract the gain and energy resolution of the detector prototypes.

3.2. Data Taking Methodology

A typical Fe-55 spectrum from the SM triple GEM chamber prototype is shown in Figure 6 for an applied voltage of $\Delta V \sim 410$ V across each GEM foil. The Gaussian fitted peak shown in Figure 6 corresponds to the 5.9 keV X-ray photopeak, commonly referred to as the main peak. The smaller peak is the Argon escape peak, while the larger peak on the left (below ADC channel no. 190) corresponds to the pedestal, indicating that the signal is well separated from the noise level.

[2] TTL stands for Transistor–Transistor Logic. A TTL signal is defined as a digital "1" when the signal voltage lies in between 1.5 V and 5 V, and as a digital "0" when the signal voltage lies in between 0 V and 0.7 V.

[3] NIM stands for Nuclear Instrument Modules. A NIM signal is defined as a digital "1" when the signal voltage lies in between -0.8 V and -1 V, and as a digital "0" when the signal voltage is exactly 0 V.

 doi:10.20944/preprints202603.1620.v1

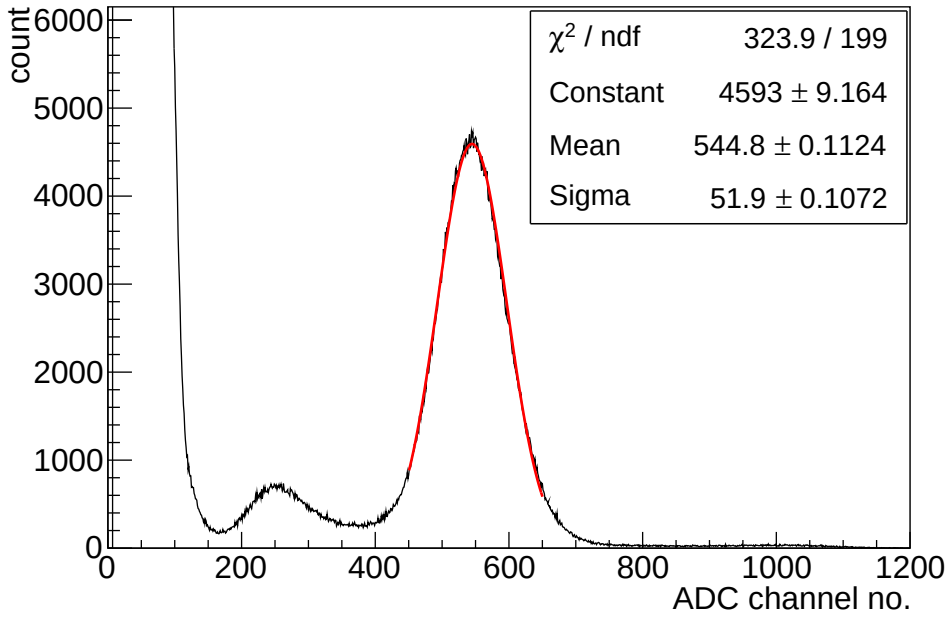

Figure 6. Typical Fe-55 spectrum from a SM triple GEM chamber operated at $\Delta V \sim 410$ V across each of the GEM foils with Ar/CO_2 gas mixture in 70/30 volume ratio.

Gain and energy resolution of the detector have been calculated using the fit parameters using the following formulae;

$$gain = \frac{Output\ charge}{Input\ charge} = \frac{(mean \times CF)/(2\ \mathrm{mV/fC})}{No.\ of\ primary\ electrons \times e} \tag{1}$$

$$energy\ resolution = \frac{sigma \times 2.355}{mean} \tag{2}$$

Here, CF is the calibration factor obtained from the MCA calibration [4], which is used to convert the MCA channel number into pulse height and then normalised by the preamplifier gain (2 mV/fC) to calculate the total output charge. The number of primary electrons is calculated by assuming full energy deposition of the 5.9 keV X-ray in the drift gap and using the average energy required for electron-ion production in the used gas mixture. For an Ar/CO_2 gas mixture in a 70/30 volume ratio, the average number of primary electrons produced by the 5.9 keV X-ray is 212 [5]. The count rate is measured using a NIM scaler after applying an appropriate threshold to suppress background contributions.

To study the charging-up phenomenon in the triple GEM detector prototypes, spectra using the Fe-55 source were recorded over different time intervals, depending on the requirements of the study. In some cases, spectra were recorded continuously, with each spectrum corresponding to a duration of 30 seconds to 1 minute, while in other cases, 1 minute spectra were recorded at intervals of 5–10 minutes. Since the gain of gaseous detectors also varies with ambient temperature and pressure, an in house built data logger was used to monitor these environmental parameters [77]. The gain and energy resolution were normalised to eliminate variations arising from changes in ambient temperature and pressure. Details of the normalisation procedure are reported in Ref. [55,59]. In Figure 7, a typical variation of the normalised gain with time is shown for the SM triple GEM chamber prototype.

[4] Pulse height (in V) = 0.1428 + MCA channel number × 0.0014

[5] Estimation for the number of primary electron generation in a typical gas mixture: $N_0 = E_\gamma \left(\frac{\%Ar}{W_{Ar}} + \frac{\%CO_2}{W_{CO_2}} \right)$, where $W_{Ar} \approx 26$ eV and $W_{CO_2} \approx 33$ eV are the average energies needed to produce one electron–ion pair in the respective gases, and E_γ is the photon energy (5.9 keV for the Fe-55 source).

 doi:10.20944/preprints202603.1620.v1

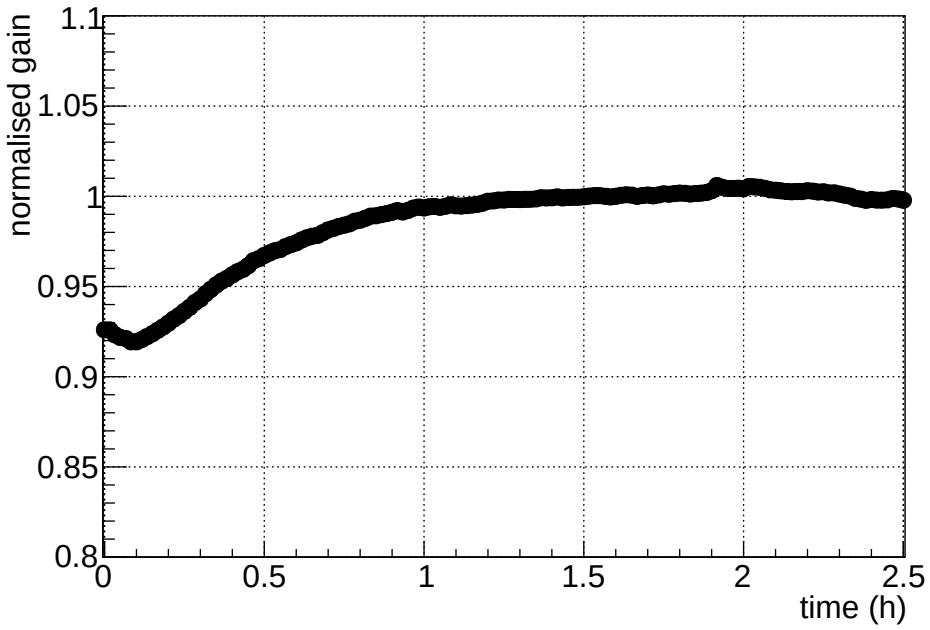

Figure 7. Normalised gain variation with time for an SM triple GEM detector. The gain normalisation is performed to eliminate the ambient temperature and pressure variation effects.

The initial hour in Figure 7 shows the gain variation due to the charging-up effect, after which the gain reaches a constant value. The normalised gain is fitted with an exponential function of the form:

$$normalised\ gain\ =\ p0\left(1-p1e^{\left(\frac{-t}{p2}\right)}\right) \tag{3}$$

where $p0$ and $p1$ are constants, t is the measurement time in hours, and $p2$ represents the charging-up time, analogous to the charging behaviour of an RC circuit [45,49].

Charging-up times were extracted for both the DM and SM GEM detector prototypes at different irradiation rates and detector gains. G-10 collimators were used to vary the irradiation rate. In the following sections, the results obtained from the DM and SM triple GEM chamber prototypes are summarised.

4. Results & Discussions

This section summarises the dependence of charging-up behaviour on irradiation rate and detector gain for both DM and SM triple GEM detector prototypes tested with an Ar/CO_2 gas mixture (70/30 volume ratio) in continuous flow mode. The same Fe-55 source was used both to record the spectra and irradiate the chamber. The X-ray rate incident on the detector was varied using G-10 collimators of different diameters. Ambient temperature and pressure were recorded continuously using a data logger [77].

4.1. Observations from the DM Triple GEM Detector Prototype

Figure 8 shows the variation of gain and the ratio of ambient temperature (T) to pressure (p) with time for three different X-ray rates, namely 1 kHz in the left (Figure 8 (a)), 10 kHz in the middle (Figure 8 (b)) and 90 kHz in the right (Figure 8 (c)).

 doi:10.20944/preprints202603.1620.v1

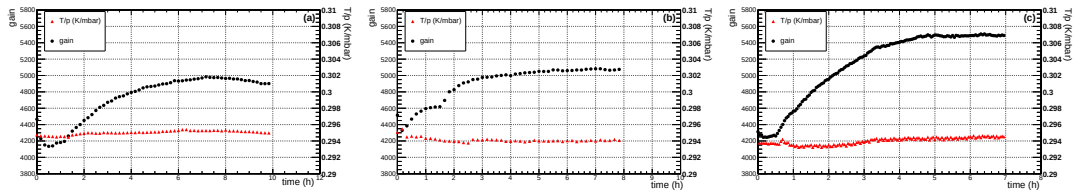

Figure 8. Variation of gain and T/p as a function of time for the DM triple GEM chamber prototype for three different X-ray rates (fluxes), namely (a) 1 kHz (0.08 kHz/mm^2), (b) 10 kHz (0.2 kHz/mm^2), and (c) 90 kHz (3.2 kHz/mm^2). The chamber was operated at -4200 V ($\Delta V \sim 390$ V), and the measurements were performed at three different positions on the active area of the chamber. The error bars are smaller than the marker size [45].

X-rays with rates of 1 kHz, 10 kHz, and 90 kHz were directed onto the detector regions of 13 mm^2, 50 mm^2, and 28 mm^2, respectively, using different collimators. This configurations correspond to particle fluxes of 0.08 kHz/mm^2, 0.2 kHz/mm^2, and 3.2 kHz/mm^2, respectively. All measurements were performed with an applied HV of -4.2 kV, resulting a potential difference of $\Delta V \sim 390$ V across each GEM foil. Due to the applied voltage, the drift, transfer, and induction fields were set to 2.3 kV/cm, 3.5 kV/cm, and 3.5 kV/cm, respectively by the divider circuit as shown in Figure 4 (left). In each case, data taking started immediately after applying the HV and positioning the radioactive source over the detector's active region. Energy spectra were recorded every 10 minutes for the 1 kHz and 10 kHz rates and every 3 minutes for the 90 kHz rate. From Figure 8, it is clear that the detector gain exhibits an initial decline during the first few minutes of operation, followed by a gradual increase over several hours before reaching a stable plateau. The early reduction in gain is attributed to the capture of primary electrons on the polarised Kapton surfaces of the GEM foils. Since dielectric polarisation develops over a finite timescale, a transient decrease in gain was observed when both the high voltage and irradiation were initiated simultaneously. This was subsequently followed by a pronounced rise in gain during the first few hours, associated with the known charging-up phenomenon. The final saturated gain values differ slightly among the three measurements, as they were conducted at different positions on the detector. A spatial gain variation of approximately ∼10% (RMS) over the active area of the chamber has been reported in Ref. [56]. For all measurements, the gain exhibits saturation after an initial increase during the first few hours. To remove the influence of ambient temperature and pressure fluctuations, the gain was further normalised with respect to the T/p ratio. For the T/p correction, the saturated gain measured after six hours of continuous operation was used as the reference point, where gain variations are dominated primarily by T/p effects and not by the charging-up phenomenon.

The time evolution of the normalised gain fitted using eqn. 3 is shown in Figure 9 for X-ray irradiation rates of (a) 1 kHz (left), (b) 10 kHz (middle), and (c) 90 kHz (right), corresponding to fluxes of 0.08 kHz/mm^2, 0.20 kHz/mm^2, and 3.20 kHz/mm^2, respectively. For the fitting, data from the initial 20 minutes were not included in the fit, as this interval is influenced by both dielectric polarisation and early stage charging-up effects. After this transient period, the charging-up process dominates the gain evolution and is modelled using eqn. 3 to extract the associated time constant. In Figure 8 (b), a small change in the slope of the gain curve is noticeable between approximately 1 and 2 hours of operation. This feature results from the combined action of two competing mechanism: charging-up, which tends to increase the gain, and decrease in T/p ratio, which tend to reduce the gain. The superposition of these opposing effects leads to a change in the slope, a behaviour that is also observed in Figure 9 (b).

 doi:10.20944/preprints202603.1620.v1

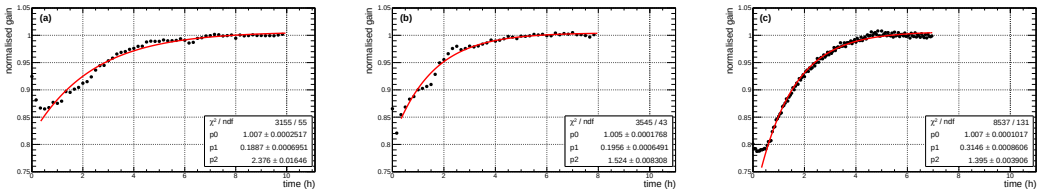

Figure 9. Variation of normalised gain with time for the DM triple GEM chamber prototype for three different X-ray rates (fluxes), namely (a) 1 kHz (0.08 kHz/mm^2), (b) 10 kHz (0.2 kHz/mm^2), and (c) 90 kHz (3.2 kHz/mm^2). The chamber was operated at -4200 V ($\Delta V \sim 390$ V). The error bars are smaller than the marker size [45].

To investigate whether the short term reduction in gain during the initial minutes of operation was attributable to the dielectric polarisation, an additional measurement was conducted in which the HV was applied continuously for 24 hours before beginning data acquisition. The detector was operated at -4.1 kV, corresponding to a voltage difference (ΔV) of approximately 382 V across each of the GEM foils. Under these conditions, the drift, transfer, and induction fields were set to 2.3 kV/cm, 3.4 kV/cm, and 3.4 kV/cm, respectively by the voltage divider circuit (Figure 4). The chamber was exposed to X-rays from the Fe-55 source at a rate of 1 kHz over a 13 mm^2 area on the detector. Data collection commenced immediately after positioning the source. The time dependance of gain, T/p, and normalised gain are presented in Figure 10 (a) and (b), respectively.

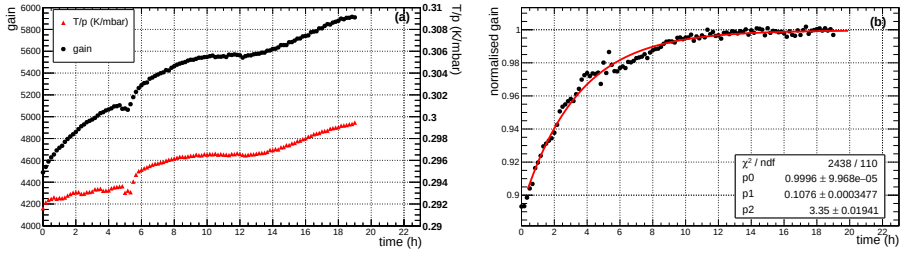

Figure 10. Variation of (a) gain, T/p and (b) normalised gain as a function of time for 1 kHz X-rays (0.08 kHz/mm^2) irradiating the chamber. The measurement was carried out at an HV of -4.1 kV, which corresponds to $\Delta V \sim 382$ V across each GEM foil. The HV was kept on for 24 hours before the first measurement with the Fe-55 X-ray source. The error bars are smaller than the marker size [45].

The data were stored at intervals of 10 minutes, with each spectrum recorded for 1 minute. It is evident that no initial reduction in gain was noticed.

Since the charging-up process is driven by charge accumulation on the GEM hole walls, it depends on the incident radiation flux. An increased flux accelerates the charging process, a trend that is clearly evident in the present measurements. From Figure 8, the charging-up time constants for 1 kHz, 10 kHz, and 90 kHz operation are found to be 2.38 ± 0.02 h, 1.52 ± 0.01 h, and 1.40 ± 0.01 h, respectively. From Figure 10, the charging-up time constant for 1 kHz X-rays is found to be 3.35 ± 0.02 h. A direct comparison between the charging-up time constants obtained from Figure 10 (b) and from Figure 9 (a) is inappropriate, as the measurements were carried out at different applied high voltages. The charging-up times, corresponding X-ray fluxes, and voltages across the GEM foils are summarised in Table 1.

 doi:10.20944/preprints202603.1620.v1

Table 1. Summary of the extracted charging-up times for the DM triple GEM chamber prototype at different irradiation rates from an Fe-55 source, for a fixed applied voltage of −4200 V [45].

Applied voltage (V)	Voltage across each GEM foil ΔV (V)	Electric field strength (kV/cm)	Flux (kHz/mm^2)	Saturated gain	Charging-up time (h)
−4200	∼390	Drift field: 2.3	∼0.08	∼4900	2.38 ± 0.02
		Transfer field: 3.5	∼0.20	∼5100	1.52 ± 0.01
		Induction field: 3.5	∼3.20	∼5500	1.40 ± 0.01

4.2. Observations from the SM Triple GEM Detector Prototype

Detailed investigation has been carried out on a SM triple GEM detector prototype to study the effect of dielectric polarisation as a function of incident particle rate and to further characterise the charging-up behaviour using the same Fe-55 source. A uniformity scan in terms of gain, energy resolution, and count rate of the prototype over its active area was also performed before and after charging-up of the GEM foils.

4.2.1. Effect of Dielectric Polarisation

To investigate the initial dielectric polarisation effects, spectra recording was initiated immediately after HV reached its designated operating value and the radioactive source was positioned at a particular location on the chamber.

As noted previously, the same Fe-55 source was employed for both irradiating the detector and for acquiring the corresponding X-ray spectra. To evaluate the influence of the applied high voltage and irradiation rate on the early stage dielectric polarisation, spectra were recorded under various HV and collimator configurations. Each spectrum was acquired over a duration of 20 seconds, with no time gap between successive measurements.

The specific HV settings used for this study, together with the corresponding voltage difference (ΔV) across each GEM foil, the average saturated gain, and the electric field strengths in the drift, transfer, and induction regions, are summarised in Table 2. A reduction in gain during the initial minutes of operation, similar to that observed for the DM triple GEM chamber, was also observed in these measurements. Figure 11 presents the time evolution of the gain for an X-ray flux of approximately 0.14 kHz/mm^2 at an applied high voltage of $-5100\ V$. During the first 20 minutes of data taking, fluctuations in the ambient temperature to pressure (T/p) ratio remained below 1% for all configurations. Given the minimal variation, no T/p correction was applied over this initial time interval.

Table 2. Summary of the voltage settings used to study the charging-up effect on the SM triple GEM detector prototype using a Fe-55 source [44].

Applied voltage (V)	Voltage across each GEM foil ΔV (V)	Saturated gain	Drift field (kV/cm)	Transfer field (kV/cm)	Induction field (kV/cm)
−5085	∼409	∼12950	∼2.4	∼3.6	∼3.6
−5100	∼410	∼13600	∼2.4	∼3.7	∼3.7
−5115	∼411	∼14300	∼2.4	∼3.7	∼3.7

 doi:10.20944/preprints202603.1620.v1

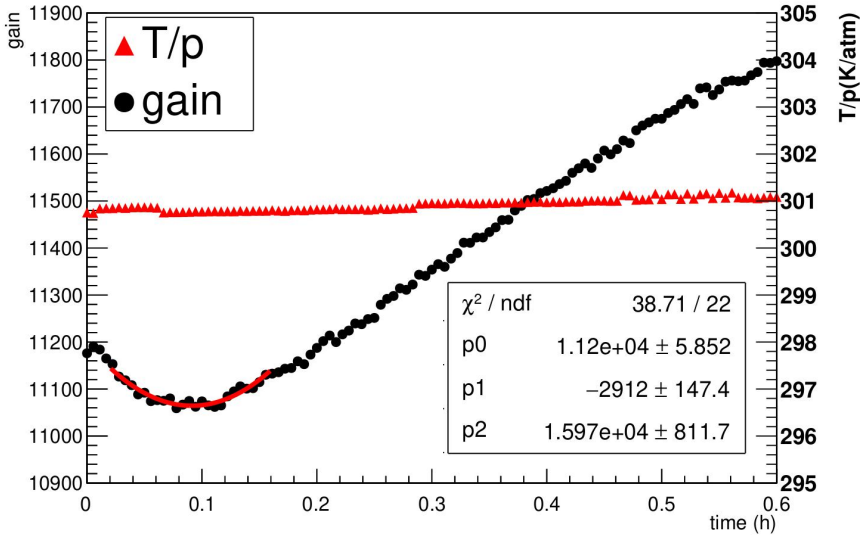

Figure 11. Variation of the gain and T/p (K/atm) as a function of time at an HV of −5100 V. The initial decrease in gain due to the polarisation effect is fitted with a 2^{nd} degree polynomial. The error bars are smaller than the marker size [44].

To determine the time interval over which the gain exhibits an initial decrease, the gain evolution was fitted with a second-order polynomial using the χ^2 minimisation method implemented in the CERN ROOT framework. From the fitted parameters, the ratio $p1/2p2$ gives the position of the minimum. The resulting fit, together with the corresponding χ^2 value, is presented in Figure 11. This fitting procedure was applied to all gain and irradiation rate configurations in order to extract the duration of the initial decrease attributed to dielectric polarisation, prior to the subsequent increase caused by the charging-up process. The extracted time intervals (in hours), corresponding to different ΔV settings and irradiation fluxes, are summarised in Table 3.

Table 3. Extracted time scales (in hours) describing the early stage gain reduction for different ΔV configurations and irradiation rates in the SM triple GEM chamber prototype [44].

Voltage across each GEM foil (V)	Flux (kHz/mm^2)	time (h)
∼409	∼0.04	0.13 ± 0.02
	∼0.14	0.11 ± 0.01
	∼0.42	0.12 ± 0.01
	∼7.78	0.13 ± 0.01
∼410	∼0.04	0.12 ± 0.02
	∼0.14	0.10 ± 0.01
	∼0.42	0.10 ± 0.01
	∼7.78	0.10 ± 0.01
∼411	∼0.04	0.13 ± 0.02
	∼0.14	0.09 ± 0.01
	∼0.42	0.08 ± 0.01
	∼7.78	0.08 ± 0.01

Figure 12 illustrates the dependence of the initial gain decrease duration on the irradiation rate. The data have been fitted with a linear function to quantify the observed trend. The extracted time interval associated with the early stage gain reduction due to dielectric polarisation shows an inverse correlation with the voltage applied across the GEM foil, as indicated by the slope parameter $p1$ of the fit. In addition, a dependence of the polarisation behaviour on the irradiation rate is evident, as

 doi:10.20944/preprints202603.1620.v1

shown in Figure 13. Specifically, the magnitude of $p1$, which represents the rate at which the initial gain decrease time changes with ΔV, increases with increasing irradiation rate.

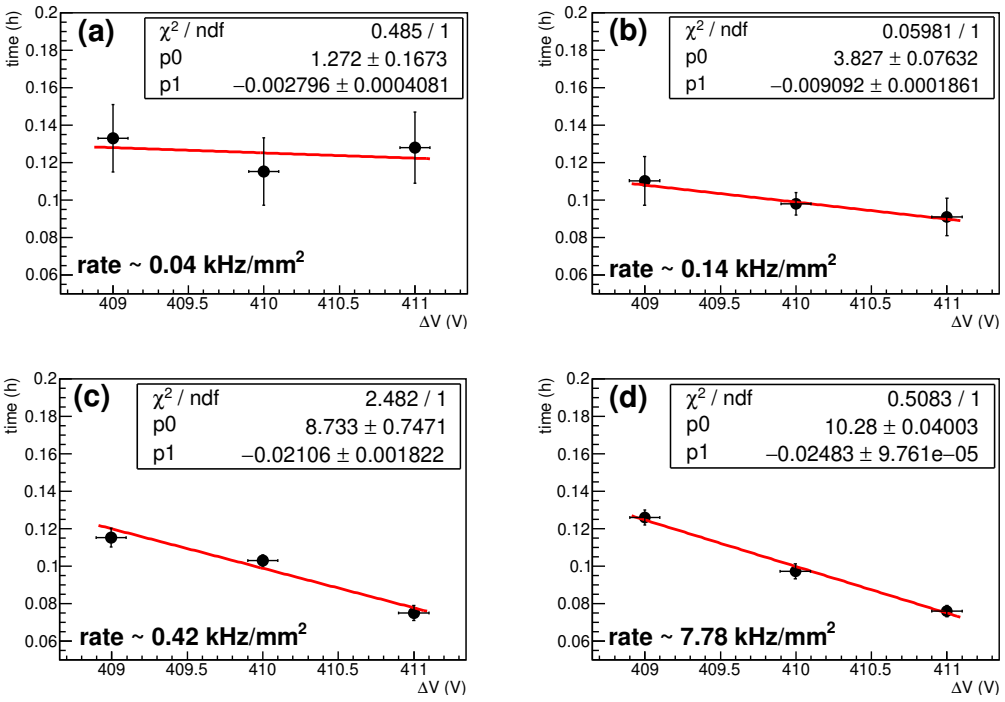

Figure 12. Dependence of the duration of the initial gain reduction on the voltage applied across each GEM foil (ΔV) for different irradiation rates [44].

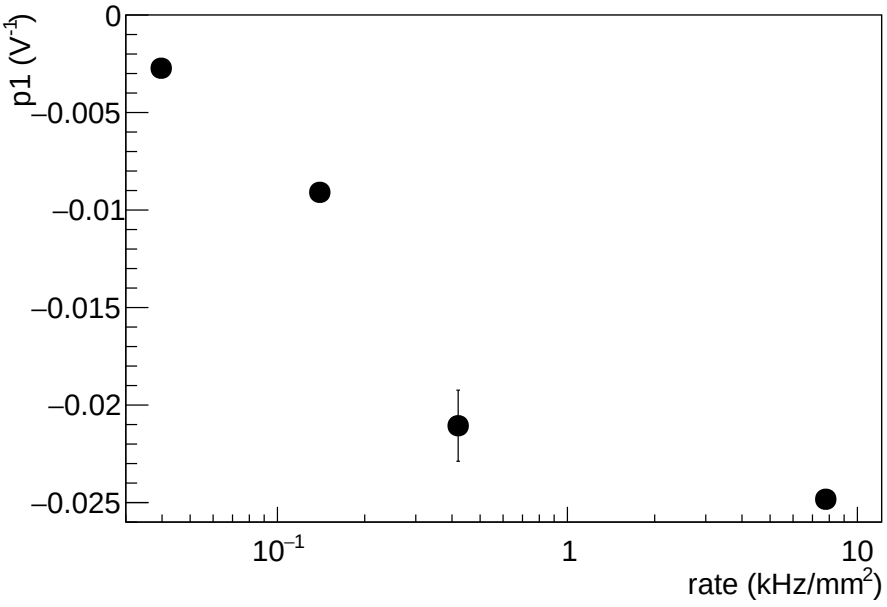

Figure 13. Slope ($p1$) as a function of the incident radiation flux per unit area [44].

4.2.2. Charging-Up Effect

To observe only the charging-up effect (excluding the dielectric polarisation contribution), the HV was switched on for approximately ∼60 minutes prior to the start of the measurement to ensure that dielectric polarisation of the GEM foils had stabilised.

 doi:10.20944/preprints202603.1620.v1

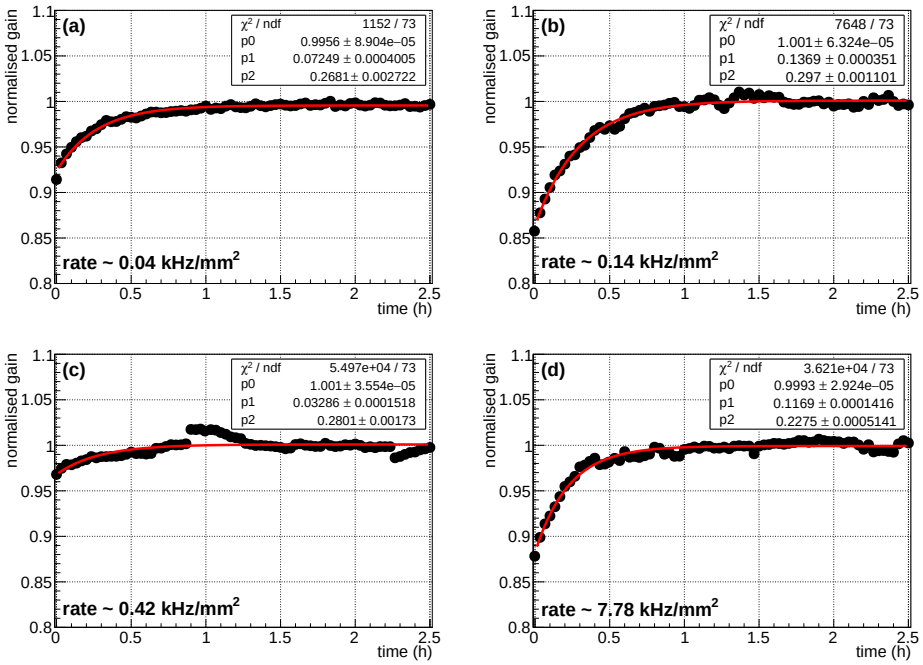

Figure 14. Normalised gain as a function of time (in hours) for various irradiation rates, recorded at an operating voltage of $-5085\ V$ ($\Delta V \sim 409$ V). The error bars are smaller than the marker size [44].

After this stabilisation period, measurements were initiated immediately after placing the Fe-55 X-ray source on the chamber. The spectra were recorded for 60 seconds at intervals of 120 seconds and analysed to obtain the detector gain. The gain was normalised to eliminate variations due to ambient temperature and pressure. In Figure 15, the variation of the normalised gain as a function of time (in hours) at an HV of -5085 V is shown for different irradiation rates. The charging-up time was found to vary between 0.2 and 0.4 hours, depending on the irradiation rate. The details of the charging-up time, irradiation rate, and saturated gain are listed in Table 4.

Table 4. Summary of the voltage across each GEM foil, corresponding saturated gain, X-ray flux, and extracted charging-up time for the SM triple GEM detector prototype [44].

Voltage across each GEM foil (V)	Flux (kHz/mm^2)	Saturated gain	Charging-up time (h)
∼409	∼0.04	∼13000	0.27 ± 0.01
	∼0.14	∼11800	0.30 ± 0.01
	∼0.42	∼12600	0.28 ± 0.01
	∼7.78	∼12200	0.23 ± 0.01
∼410	∼0.04	∼13800	0.29 ± 0.01
	∼0.14	∼13700	0.35 ± 0.01
	∼0.42	∼13500	0.41 ± 0.01
	∼7.78	∼13400	0.34 ± 0.01
∼411	∼0.04	∼14500	0.19 ± 0.01
	∼0.42	∼14000	0.44 ± 0.01
	∼7.78	∼12200	0.19 ± 0.01

 doi:10.20944/preprints202603.1620.v1

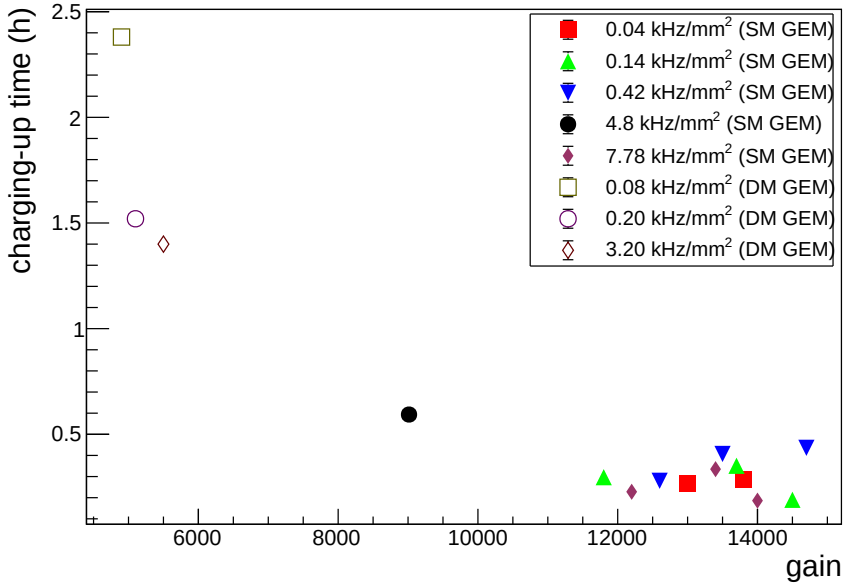

Figure 15. Charging-up time (hours) as a function of gain for the DM and SM triple GEM chamber prototypes at different irradiation rates from the Fe-55 X-ray source. The error bars are smaller than the marker size.

It was observed that, in general, with increasing irradiation rate or increasing detector gain, the rate of charge accumulation inside the GEM holes increases, thereby reducing the charging-up time. In Figure 15, a summary plot of the charging-up time is shown as a function of detector gain for both DM and SM triple GEM chambers at different X-ray rates investigated by our group.

4.2.3. Uniformity in Performance of the SM Triple GEM Chamber With and Without Charged-Up GEM Foils

Since the charging-up phenomenon introduces a time dependent variation in the chamber gain, it is important to evaluate the spatial uniformity of the detector response across the active area, both considering and neglecting the influence of charging-up. The 10 cm $\times$ 10 cm active region of the SM triple GEM chamber was segmented into a 4 $\times$ 4 grid for this study. To assess the uniformity of detector performance, the radioactive source was mounted on a G-10 collimator, which was sequentially positioned at predefined locations within the active area.

Two distinct measurement procedures were employed. In the first approach, the high voltage was applied for approximately 60 minutes prior to data acquisition. Once the source was positioned on the detector, data collection began immediately. X-ray spectra were recorded for a duration of 1 minute at each location, after which the source and collimator were manually shifted to the next grid position. Because the irradiation time at each point was limited, the GEM foils did not reach a fully charged-up state. Consequently, the results obtained under these conditions correspond to measurements performed with effectively uncharged GEM foils.

Figure 16 presents the spatial distributions of gain, energy resolution, and count rate across the scanned region for a voltage difference (ΔV) of $\sim$ 402.7 V across each GEM foil. The observed variations are about 10% for both gain and count rate, while the energy resolution exhibits a variation of approximately 15%.

 doi:10.20944/preprints202603.1620.v1

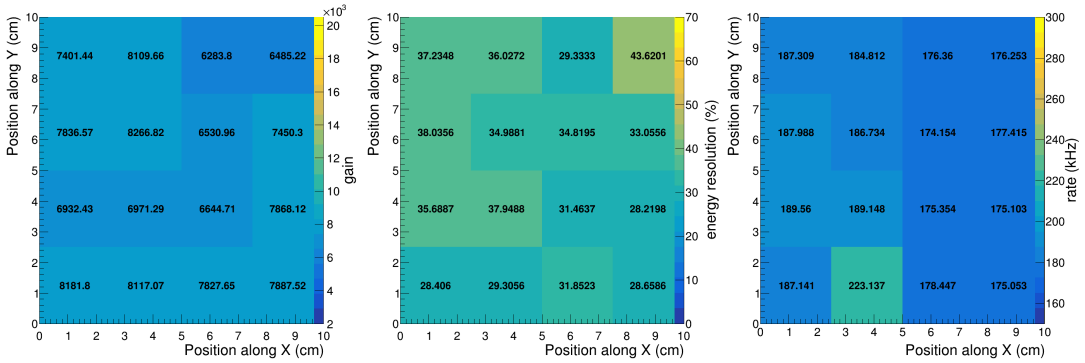

Figure 16. Uniformity measurements of gain (left), energy resolution (middle), and count rate (right) over the 10 cm $\times$ 10 cm active region of the SM triple GEM chamber, recorded at ΔV of $\sim$ 402.7 V across each of the GEM foils [46].

In the second measurement approach, the high voltage was applied and the radioactive source was positioned on the detector immediately after the voltage reached its designated operating value. Data acquisition commenced without any delay once the source was placed on the chamber. Energy spectra were recorded at 30 second intervals with no gaps between successive measurements. To account for environmental influences, the recorded data were normalised to remove the dependence of ambient temperature and pressure variations on gain and energy resolution of the chamber. The time evolution of the normalised gain was then fitted using the exponential model described in eqn. 3 to determine the charging-up time constant. Figure 17 presents the spatial distribution of the extracted charging-up times across the scanned 10 cm $\times$ 10 cm active region of the SM triple GEM detector operated at an applied high voltage of -5075 V. The average charging-up time was found to be 0.76 ± 0.08 h, with a corresponding standard deviation of 0.33 ± 0.06 h.

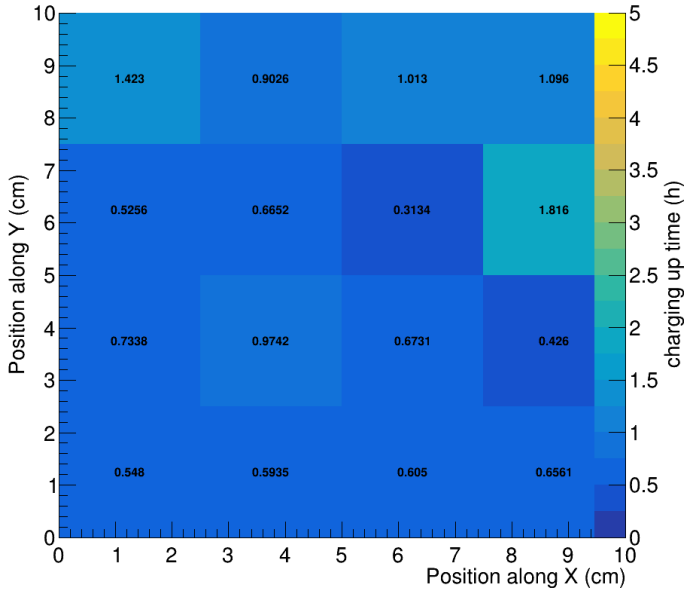

Figure 17. Charging-up time measured over the scanned 10 cm $\times$ 10 cm region of the SM triple GEM chamber at an applied voltage of -5075 V, which corresponds to ΔV of $\sim$ 402.7 V across each GEM foil [46].

To evaluate the variation in gain, energy resolution, and count rate after the charging-up process was complete, the gain and energy resolution were measured after approximately $\sim$150 minutes of continuous exposure of the chamber to the Fe-55 X-ray source, while the count rate was recorded simultaneously using the NIM scaler. The corresponding distributions of gain, energy resolution,

 doi:10.20944/preprints202603.1620.v1

and count rate across the scanned region, with the GEM foils in a charged-up state, are presented in Figure 18.

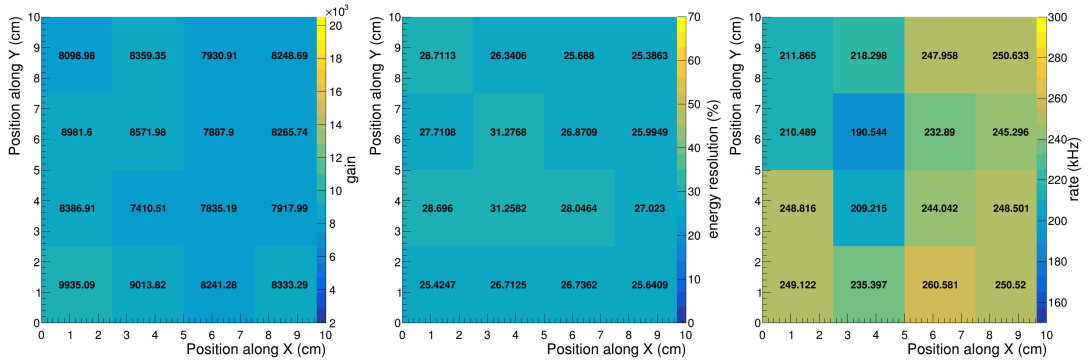

Figure 18. Uniformity scan in terms of gain (left), energy resolution (middle), and count rate (right) over the active area (10 cm $\times$ 10 cm) of the SM triple GEM chamber under investigation with charged-up GEM foils. The voltage across each GEM foil was kept constant at $\Delta V \sim 402.7$ V [46].

Across the scanned region, variations of approximately 10% were observed in gain, energy resolution, and count rate. As expected, the overall uniformity of the detector, evaluated in terms of these parameters, remained essentially unchanged after the completion of the charging-up process. The primary difference between the two cases was an increase in the absolute gain following charging-up. This enhancement in gain also led to an improvement in the energy resolution. The average gain and energy resolution measured with uncharged GEM foils were 7375 ± 171.5 and $33.31 \pm 1.08\%$, respectively. After the foils reached a charged-up state, these values increased to 8325 ± 139.1 for the gain and improved to $26.94 \pm 0.48\%$ for the energy resolution. A corresponding increase in the count rate was also observed, with mean values of 184.0 ± 2.9 kHz prior to charging-up and 234.6 ± 4.9 kHz after charging-up.

Figure 19 presents the ratios of gain, energy resolution, and count rate obtained with charged GEM foils relative to those measured with uncharged foils. The sixteen points along the X-axis correspond to the different regions of the chamber that were scanned during the uniformity study. The results indicate that both gain and count rate are systematically higher when the GEM foils are in a charged-up state. In addition, an improvement in energy resolution is observed after the completion of the charging-up process. Given that the chamber was irradiated with an Fe-55 source emitting X-rays at a constant rate, the increase in measured gain suggests an enhancement in the effective detection efficiency following charging-up. The reduced spread in energy resolution observed with charged GEM foils may be attributed to improved stabilisation of the detector response.

 doi:10.20944/preprints202603.1620.v1

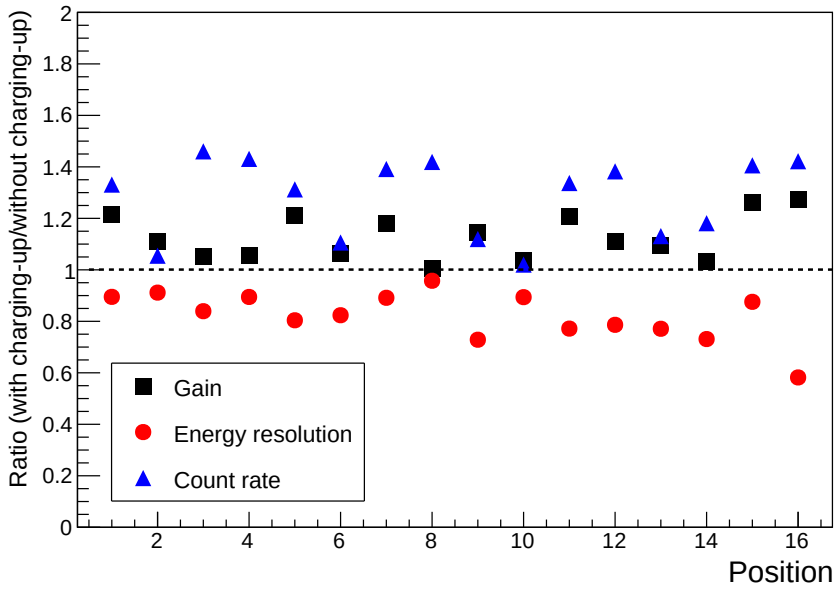

Figure 19. Comparison of gain, energy resolution, and count rate ratios obtained before and after charging-up at sixteen locations across the SM triple GEM chamber. The error bars are smaller than the marker size [46].

Several other groups have reported similar observations regarding the charging-up phenomenon in GEM detectors. R. Bouclier *et al.* [47] reported earlier studies in which a GEM mesh was added as a pre-amplification element to multi-wire and micro-strip chambers. A moderate upward shift in gain was observed, which reached a constant value with a time constant that depended on the irradiation rate. It was also shown that, upon suspending the irradiation, the gain returned to its original value with a time constant of several hours. These measurements were carried out using very low irradiation rates ($\sim$15 Hz/mm^2). The study further reported a correlation between the extent of the gain shift and the geometry of the GEM mesh. It was also demonstrated that adding a small, controlled amount of water vapour to the gas mixture helped to reduce the charging-up effect by lowering the inter-electrode resistivity. However, this approach was discouraged, as it increases the likelihood of electrical conductivity between the anode and cathode, potentially raising the spark probability in MPGD technologies.

The article by B. Azmoun *et al.* (B. Azmoun *et al.*, [40] reported charging-up studies on GEM foils manufactured by different vendors and investigated the effects of irradiation rate and water content in the active gas volume on the charging-up behaviour of the chamber. This study concluded that the amount of exposed polyimide within the GEM holes is one of the primary factors influencing the magnitude of the charging-up effect observed for a given foil. Another study by J. Benlloch *et al.* [48] reported the influence of GEM hole geometry on the charging-up effect.

P. Hauer *et al.* [49] investigated charging-up effects in a DM single GEM detector prototype for different X-ray irradiation rates. In their study, a drift gap of 25.7 mm and an induction gap of 2.25 mm were employed. Both the current from the readout plane, measured using an X-ray generator, and energy spectra, recorded using an Fe-55 source, were analysed to characterise the charging-up behaviour.

Beyond the context of tracking detectors for high and intermediate energy nuclear physics experiments, the work by M. Chernyshova *et al.* [50] explored the implications of the charging-up effect on GEM chambers considered for plasma radiation monitoring applications.

The results from all these studies are in good agreement with the observations obtained from the investigations carried out by the authors using triple GEM chamber prototypes [54–57].

 doi:10.20944/preprints202603.1620.v1

5. Monte-Carlo Simulation Efforts

There have been significant efforts aimed at modelling the charging-up effect in GEM detectors, or more generally in systems where the active area of a detector contains dielectric material and is exposed to external irradiation within a gaseous medium. One of the early efforts was carried out by V. Tikhonov and R. Veenhof and reported in Ref. [51]. This work discussed the development of GEM simulation methods that could be used for detector optimisation. The study described the use of the Maxwell [78] and Garfield [79] simulation packages to model GEM chambers with different geometrical parameters, including the inner and outer diameters of the holes, the thickness of the dielectric, the pitch structure, and the thickness of the copper cladding on the Kapton foil, for an Ar/CO_2 gas mixture in a 70/30 ratio. The simulation results were found to be in good agreement with experimental data. The charging-up effect was modelled using an RC network, with the time constant governed primarily by the capacitance and resistivity of the surface of the GEM holes under study. However, no detailed dynamic electric fields inside and around the GEM holes were implemented in this study.

M. Alfonsi *et al.* [42] reported simulation studies of the dielectric charging-up effect in a standard GEM detector [6]. In this work, the authors employed the Ansys [80] software package to generate electric field maps inside and around the GEM holes using the finite element method (FEM), in conjunction with the Garfield [81] package for an Ar/CO_2 gas mixture in a 70/30 ratio. The charging-up effect was incorporated into the simulations through an iterative procedure. The distribution of charge on the Kapton surface inside the holes was approximated by exploiting the axial symmetry and bi-conical geometry of the GEM holes. At each iteration step, the electric field was recalculated using the updated charge configuration on the top and bottom halves of the Kapton foil, where the hole was divided into two regions and the charge distribution was assumed to be uniform at the beginning of each iteration. The study also reported the fraction of electrons terminating on different GEM layers in the detector and its evolution as a function of time. The authors concluded that an accurate simulation of the charging-up effect in GEM-based detectors is essential, as it enables a more detailed investigation of the underlying processes and provides a pathway toward optimising detector geometry to control and mitigate charging-up effects.

P. M. M. Correia *et al.* [43] reported a dynamic method for charging-up calculations in GEM based detectors. In this work, the authors developed and discussed two different approaches for modelling charge accumulation in GEM detectors. Simulations were carried out using a standard GEM foil geometry with a Ar/CO_2 gas mixture in a 70/30 ratio. Ansys [80] was used to generate the electric field maps, while Garfield++ [82] was employed to simulate the drift and transport properties of electrons and ions in the gas medium. Two iterative methods, namely the constant step method and the dynamic step method, were introduced, differing only in the manner in which the electric field map is updated to account for charge accumulation on the insulating (Kapton) surface. In the constant step method, a fixed number of primary avalanches ($\sim 10^4$) were simulated, and the resulting surface charge density was calculated. The electric field was then updated according to the new charge distribution, and the process was repeated until the extracted gain stabilised, requiring many iteration steps. In contrast, the dynamic step method employed a variable step size that depended on the number of charges deposited per avalanche on the insulator surface. This approach was reported to result in faster computation, while both methods exhibited similar behaviour. The temporal evolution of the gain obtained from the simulations was found to agree well with experimental data, however, the absolute gain values were overestimated compared to measurements. The authors attributed this discrepancy to limitations in the implementation of charge mobility, electric field calculations, and possible fabrication imperfections in the GEM foils under test, which could affect the measured gain.

A relatively recent study by J. Jiang *et al.* [83] reported the development of a model in which charge transport within the GEM insulator itself was argued to play a significant role in the charging-up

[6] The thickness of the copper-clad Kapton foil is 50 μm, and the GEM holes have a bi-conical shape with internal and external diameters of 50 μm and 70 μm, respectively, arranged in a hexagonal pitch pattern of 140 μm.

 doi:10.20944/preprints202603.1620.v1

characteristics of GEM based detectors. Accordingly, the authors proposed a model that included charge transport in the bulk of the GEM insulator (Kapton), which they referred to as a discharge process, and compared the simulation results with data available in the literature. They concluded that the charging-up trends obtained from simulations incorporating this discharge process were consistent with previous studies, however, they also noted that the formulation of the discharge process could be further improved and reported ongoing efforts in this direction.

Several other studies have also addressed the simulation of charging-up effects. For example, P. Bhattacharya *et al.* [84] reported on the development and comparison of different models to simulate the charging-up effect, space-charge formation, and discharge processes in GEMs and Thick GEMs (THGEMs). In addition, M. Pitt *et al.* [85], and G. Song *et al.* [86] reported simulation studies on gain stability in THGEM detectors, including the effects of charging-up.

6. Summary & Outlook

This article summarises the investigations carried out by the authors on DM and SM triple GEM chamber prototypes using a Fe-55 source both as the radiation source and for recording the energy spectra. The charging-up time is defined by drawing an analogy with the charging process of an RC network, and the dependence of charging-up time on detector gain and irradiation rate is reported. In all studies, the relative increase in gain is observed to be less than 30%. A brief overview of investigations of the charging-up effect performed by different groups is also included. Overall, the results from these studies show qualitative agreement with one another. There are, however, a few studies in which a decreasing trend in gain due to the charging-up effect has been observed [87,88].

A brief summary of Monte Carlo simulation efforts by different groups is also presented. Significant efforts are currently ongoing to improve modelling approaches for reproducing the charging-up effect in GEM based detectors using various iterative methods.

The charging-up effect in a triple GEM chamber is a convoluted process and therefore requires more detailed investigation. Most existing studies, both experimental and simulation based, reported in the literature focus on single-GEM detectors. Consequently, it would be particularly interesting to study and disentangle the individual contributions of charging-up from each GEM foil to the final detector response in a triple GEM configuration. In addition, studying the role of electric fields in the different regions of the GEM chamber would be another important direction, as it could provide further insight into how the field strengths between GEM foils influence charge densities inside the GEM holes at different stages, which in turn affect the overall charging-up behaviour in a triple GEM chamber.

As the use of GEM-based detectors is becoming increasingly popular in applications such as medical imaging, space based experiments, and muon tomography, where particle rates are typically lower than those encountered in high and intermediate energy nuclear physics experiments, it is particularly important to understand charging-up effects that influence detector performance. In particular, gain variations due to charging-up directly impact the detection efficiency of the chamber.

Therefore, continued efforts to improve simulation frameworks for accurately modelling the charging-up effect, together with more controlled experimental studies to obtain additional data on the underlying charging mechanisms in GEM based detectors, are of paramount importance for optimising the geometry and design of GEM based detector systems.

Author Contributions: Conceptualization: S. Chatterjee and S. Biswas; Methodology: S. Chatterjee, A. Sen and S. Biswas; Software: S. Chatterjee; Validation: S. Chatterjee, A. Sen, S. Das and S. Biswas; Formal analysis: S. Chatterjee; Investigation: S. Chatterjee; Resources: S. Das and S. Biswas; Data curation: S. Chatterjee; Writing—original draft preparation: S. Chatterjee; Writing—review and editing: S. Chatterjee, S. Das and S. Biswas; Visualization: S. Chatterjee; Supervision: S. Biswas; Funding acquisition: S. Das and S. Biswas. All authors have read and agreed to the published version of the manuscript.

 doi:10.20944/preprints202603.1620.v1

Funding: This work was partially supported by the research grant SR/MF/PS-01/2014-BI from DST, Govt. of India, and by the CBM-MuCh project research grant from BI-IFCC, DST, Govt. of India. S. Biswas acknowledges support from the DST-SERB Ramanujan Fellowship, India (D.O.No.: SR/S2/RJN-02/2012).

Data Availability Statement: The data can be made available upon request. For inquiries, please contact Sayak Chatterjee (sayakchatterjee896@gmail.com) and Saikat Biswas (saikat@jcbose.ac.in).

Acknowledgments: The authors would like to thank the RD51 collaboration for support in building and initial testing of the chamber in the RD51 laboratory at CERN. We would like to thank Dr. E. Oliveri, Dr. A. Sharma, Dr. L. Ropelewski and Dr. Chilo Garabatos of CERN, Dr. C. J. Schmidt and Mr. Jörg Hehner of the GSI Detector Laboratory. Prof. Sanjay K. Ghosh, Prof. Sibaji Raha, Prof. Rajarshi Ray, and Dr. Sidharth K. Prasad of Bose Institute for valuable discussions and suggestions during the course of this work. The authors would also like to thank Dr. Arindam Sen, Dr. Shreya Roy, Ms. Krishna Nivedita G, Ms. Aayushi Paul, Mr. Shreesh Sahai and Mr. Subrata Das for their contributions during data taking and in setting up the experimental setup.

Conflicts of Interest: The authors declare no conflicts of interest. The funders had no role in the design of the study, in the collection, analyses, or interpretation of data, in the writing of the manuscript, or in the decision to publish the results.

References

1. F. Sauli, Nucl. Instr. Meth. Phys. Res. A, 386 (1997) 531
2. F. Sauli, Nucl. Instr. Meth. Phys. Res. A, 805 (2016) 2
3. A.F. Buzulutskov, Instrum. Exp. Tech. 50, 287 (2007)
4. B. Ketzer, et al., Nucl. Instr. Meth. Phys. Res. A, 535 (2004) 314
5. C. Altunbas et al., Nucl. Instr. Meth. Phys. Res. A, 490 (2002) 177
6. F. Simon, Commissioning of the GEM detectors in the COMPASS experiment, 2001 thesis, Technische Universität München
7. ALICE TPC collaboration et al., 2021 JINST 16 P03022
8. B. Ketzer, For the GEM-TPC and ALICE TPC Collaborations, Nucl. Instr. Meth. Phys. Res. A, 732 (2013) 237
9. G. Mocellin, on behalf of the CMS Muon Group, J. Phys.: Conf. Ser. 1390, 012116 (2019)
10. C. Calabria, on behalf of the CMS GEM Collaboration, Nuclear and Particle Physics Proceedings 273, 1042 (2016)
11. B. Azmoun et al., IEEE Symposium Conference Record Nuclear Science 2004, Vol. 1, 480
12. K. Gnanvo et al., Nucl. Instr. Meth. Phys. Res. A, 782 (2015) 77
13. A. K. Dubey et al., Nucl. Instr. Meth. Phys. Res. A, 718 (2013) 418
14. A. Kumar et al., 2021 JINST 16 P09002
15. J Arrington et al 2023 J. Phys. G: Nucl. Part. Phys. 50 110501
16. D.W. Higinbotham 2022 JINST 17 C02018
17. B. Azmoun et al., IEEE Transactions on Nuclear Science Vol: 63, No: 3, 2016
18. G. Alocco for the NA60+ collaboration, EPJ Web of Conferences 296, 08005 (2024)
19. M. Borysova PoS (ICHEP2022) 978
20. K. Gnanvo et al., Nucl. Instr. Meth. Phys. Res. A, 652 (2011)16
21. P. Gros et al., POS(TIPP2014) 133
22. S. D. Hunter et al., Astroparticle Physics 59, 18 (2014)
23. S. D. Pinto, Modern Physics Letters A Vol. 28, No. 13, 1340025 (2013)
24. M. Bucciantonio, and F. Sauli, Modern Phys. Lett. A, 30(17), 1540024 (2015)
25. F. Anulli et al., Nucl. Instr. Meth. Phys. Res. A, 572 (2007) 266
26. E. Tsyganov et al., Nucl. Instr. Meth. Phys. Res. A, 597 (2008) 257
27. R. M. Gutierrez et al., 2012 JINST, 7 C07007
28. Oliveira et al., United States Patent, Patent No.: US 8,597,490 B2
29. H. Keller et al., 2020 JINST 15 C06004
30. P. Roy et al., 2022 JINST 17 P03016
31. E. Brücken et al., Nucl. Instr. Meth. Phys. Res. A, 1002 (2021) 165271
32. Gaseous Electron Multiplier; https://gdd.web.cern.ch/gem
33. D. Abbaneo et al., Nucl. Instr. Meth. Phys. Res. A, 845 (2017) 298
34. S. Chatterjee et al., Nucl. Instr. Meth. Phys. Res. A, 977 (2020) 164334

 doi:10.20944/preprints202603.1620.v1

35. S. Biswas et al., Nucl. Instr. Meth. Phys. Res. A, 800 (2015) 93
36. S. Lami et al., Nuclear Physics B (Proc. Suppl.) 172, 231 (2007)
37. O. Eraldo, The forward inelastic telescope T2 for the TOTEM experiment at the LHC, PhD thesis, University of Siena
38. M. Alfonsi et al., Nucl. Instr. Meth. Phys. Res. A, 518 (2004) 106
39. M.P. Lener, Triple-GEM detectors for the innermost region of the muon apparatus at the LHCb experiment, PhD thesis (2006)
40. B. Azmoun et al., IEEE Nuclear Science Symposium Conference Record, VOL. 6, pages 3847 - 3851, (2006)
41. M. V. Nemallapudi, Master's Thesis at University of Arkansas. 2012 https://scholarworks.uark.edu/etd/533/
42. M. Alfonsi, Nucl. Instr. Meth. Phys. Res. A, 671 (2012)6
43. P. M. M. Correia et al., 2014 JINST 9 P07025
44. S. Chatterjee et al., Nucl. Instr. Meth. Phys. Res. A, 1014 (2021) 165749
45. S. Chatterjee et al., 2020 JINST 15 T09011
46. S. Chatterjee et al., Nucl. Instr. Meth. Phys. Res. A, 1049 (2023)168110
47. R. Bouclier et al., Nucl. Instr. Meth. Phys. Res. A, 396 (1997) 50
48. J. Benlloch et al., Nucl. Instr. Meth. Phys. Res. A, 419 (1998) 410
49. P. Hauer et al., Nucl. Instr. Meth. Phys. Res. A, 976 (2020) 164205
50. M. Chernyshova et al., Fusion Engineering and Design 158, 111755 (2020)
51. V. Tikhonov and R. Veenhof, Nucl. Instr. Meth. Phys. Res. A, 478 (2002) 452
52. S. Biswas, Virginia Journal of Business, Technology, and Science, 2021
53. S. Mandal et al., Nucl. Instr. Meth. Phys. Res. A, 1064 (2024) 169389
54. Sayak Chatterjee, Performance Studies of Gas Electron Multiplier Detector for the Muon Chamber of High Rate CBM Experiment at FAIR, Ph.D. Thesis, University of Calcutta, 2023
55. S. Chatterjee et al., Nucl. Instr. Meth. Phys. Res. A, 1046 (2023) 167747
56. S. Chatterjee et al., Nucl. Instr. Meth. Phys. Res. A, 936 (2019) 491
57. S. Chatterjee et al., 2023 JINST 18 C05002
58. R.P. Adak et al., 2016 JINST 11 T10001
59. S. Roy et al., Nucl. Instr. Meth. Phys. Res. A, 936 (2019) 485
60. S. Mandal et al., Proceedings of the DAE Symp. on Nucl. Phys. 68 (2024) 1111
61. S. Mandal et al., Proceedings of the DAE Symp. on Nucl. Phys. 67 (2023) 1251
62. S. Sahai et al., Proceedings of the DAE Symp. on Nucl. Phys. 66 (2022) 1186
63. A. Sen et al., 2025 JINST 20 T03007
64. A. Sen et al., Nucl. Instr. Meth. Phys. Res. A, 1045 (2023)167572
65. Arindam Sen, Development Of Resistive Plate Chamber For The CBM Experiment At FAIR And Other Application Of Radiation Detector, Ph.D. Thesis, University of Calcutta, 2023
66. S. Chakraborty et al., Proceedings of the DAE Symp. on Nucl. Phys. 69 (2025) 1265
67. A. Sen et al., Nucl. Instr. Meth. Phys. Res. A, 1024 (2022) 166095
68. A. Sen et al 2020 JINST 15 C06055
69. S. Chakraborty et al., Nucl. Instr. Meth. Phys. Res. A, 936 (2019) 424
70. S. Roy et al., Pramana J. Phys 95, 50 (2021)
71. Shreya Roy, Characterization Of Gaseous And Scintillator Detectors For High Energy Physics And Cosmic Ray Experiments, Ph.D. Thesis, University of Calcutta, 2022
72. S. Roy et al., Proceedings of the DAE International Symp. on Nucl. Phys. 63 (2018) 1046
73. S. Roy et al., Proceedings of the DAE International Symp. on Nucl. Phys. 64 (2019) 990
74. S. Roy et al., Nucl. Instr. Meth. Phys. Res. A, 936 (2019) 488
75. CERN ROOT, https://root.cern/
76. CDT CASCADE Detector Technologies GmbH, Germany, www.n-cdt.com
77. S. Sahu et al., 2017JINST 12 C05006
78. Maxwell 3-D Field Simulator, User Reference, Ansoft Corporation
79. R. Veenhof, Garfield, A Drift-Chamber Simulation Program
80. www.ansys.com
81. R. Veenhof, Nucl. Instr. Meth. Phys. Res. A, 419 (1998) 726
82. Garfield++, https://garfieldpp.web.cern.ch/
83. J. Jiang et al 2024 JINST 19 T10008
84. P. Bhatcharya et al., Nucl. Instr. Meth. Phys. Res. A, 1075 (2025) 170336

 doi:10.20944/preprints202603.1620.v1

85. M. Pitt et al 2018 JINST 13 P03009
86. G. Song et al 2020 JINST 15 P04015
87. Gabriele Croci, Study of relevant parameters of GEM-based detectors, Ph.D. Thesis (2009)
88. V. Kumar et al 2021 JINST 16 P01038